Assessment of the dynamic interactions between heart rate and arterial pressure by the cross time–frequency analysis

M Orini[1,2,3]**, P Laguna**[1,2]**, L T Mainardi**[3] **and R Bailón**[1,2]

[1] Communications Technology Group (GTC), Aragón Institute of Engineering Research (I3A),
University of Zaragoza, M de Luna 1, Zaragoza 50018, Spain
[2] CIBER de Bioingeniería, Biomateriales y Nanomedicina (CIBER-BBN), Barcelona, Spain
[3] Department of Bioengineering, Politecnico di Milano, Via Golgi 39, Milano 20131, Italy

E-mail: michele@unizar.es

Abstract

In this study, a framework for the characterization of the dynamic interactions
between RR variability (RRV) and systolic arterial pressure variability (SAPV)
is proposed. The methodology accounts for the intrinsic non-stationarity of
the cardiovascular system and includes the assessment of both the strength
and the prevalent direction of local coupling. The smoothed pseudo-Wigner–
Ville distribution (SPWVD) is used to estimate the time–frequency (TF)
power, coherence, and phase-difference spectra with fine TF resolution.
The interactions between the signals are quantified by time-varying indices,
including the local coupling, phase differences, time delay, and baroreflex
sensitivity (BRS). Every index is extracted from a specific TF region, localized
by combining information from the different spectra. In 14 healthy subjects, a
head-up tilt provoked an abrupt decrease in the cardiovascular coupling; a rapid
change in the phase difference (from 0.37 ± 0.23 to -0.27 ± 0.22 rad) and
time delay (from 0.26 ± 0.14 to -0.16 ± 0.16 s) in the high-frequency band;
and a decrease in the BRS (from 23.72 ± 7.66 to 6.92 ± 2.51 ms mmHg^{-1}).
In the low-frequency range, during a head-up tilt, restoration of the baseline
level of cardiovascular coupling took about 2 min and SAPV preceded RRV
by about 0.85 s during the whole test. The analysis of the Eurobavar data set,
which includes subjects with intact as well as impaired baroreflex, showed
that the presented methodology represents an improved TF generalization of
traditional time-invariant methodologies and can reveal dysfunctions in subjects
with baroreflex impairment. Additionally, the results also suggest the use of

non-stationary signal-processing techniques to analyze signals recorded under conditions that are usually supposed to be stationary.

Keywords: cardiovascular interactions, cross time–frequency analysis, coherence analysis, Wigner–Ville distribution, cardiovascular variability, baroreflex

S Online supplementary data available from stacks.iop.org/PM/33/315/mmedia

(Some figures may appear in colour only in the online journal)

1. Introduction

Short-term cardiovascular control involves homeostatic mechanisms for the maintenance of blood pressure, which make the blood pressure and heart rate to continuously interact. A change in the blood pressure causes a change in the heart rate through the feedback baroreceptor-cardiac reflex (baroreflex), while, in turn, a change in the heart rate causes a change in the blood pressure through feedforward mechanical effects. The assessment of baroreflex sensitivity (BRS), i.e. the change in the RR interval following a unitary change in the blood pressure, from non-invasive measurements is clinically relevant because a baroreflex impairment has been suggested to have diagnostic and prognostic relevance (Di Rienzo *et al* 2009, La Rovere *et al* 2008). Over the last 20 years, different techniques have been proposed to estimate the spontaneous BRS (Laude *et al* 2004, Pagani *et al* 1988, Vallais *et al* 2009, Robbe *et al* 1987, Barbieri *et al* 2001, Gouveia *et al* 2009). Among them, there is the cross-spectral analysis of systolic arterial pressure variability (SAPV) and RR variability (RRV) (Di Rienzo *et al* 2009, La Rovere *et al* 2008). In particular, the parameter α_B has been defined as the squared root of the ratio between the powers of the RRV and SAPV series, and it is usually defined in both the low-frequency (LF; range [0.04, 0.15 Hz]) and high-frequency (HF; range [0.15, 0.4 Hz]) spectral bands (Pagani *et al* 1988, Laude *et al* 2004). Traditionally, this parameter is estimated whenever the spectral coherence between RRV and SAPV is higher than an arbitrary threshold. Although the first methodologies to estimate spontaneous BRS are not recent (Robbe *et al* 1987, Pagani *et al* 1988, Mainardi *et al* 1997), over the last few years, the interest in improved methods has increased. Recently, much effort has been put into improving two issues: the capability of following changes under non-stationary conditions and the assessment of the causality between RRV and SAPV. However, only a few methodologies that combine non-stationary analysis and the assessment of causality have been applied in the study of cardiovascular interactions (Chen *et al* 2011). Non-stationary processing is important because in the cardiovascular system, stationarity is a rare exception rather than the rule. Recent non-stationary methods for the analysis of cardiovascular interactions are based on time-varying autoregressive models (Xiao *et al* 2005, Chen *et al* 2011), continuous and discrete wavelet transform (Kashihara *et al* 2009, Keissar *et al* 2010, Nowak *et al* 2009, Wiklund *et al* 2002) and empirical mode decomposition (de Souza Neto *et al* 2007, Gallet *et al* 2011).

The assessment of the causality is relevant because it can be used to infer which mechanism is primarily responsible for the changes observed in the signals and is necessary to assess spontaneous BRS (Porta *et al* 2011). To determine the prevalent direction of the coupling between RRV and SAPV (Nollo *et al* 2009), cross-spectral analysis has been traditionally used (Cooke *et al* 1999, Li and Jung 2000). Recently, parametric modeling (Nollo *et al* 2005, Chen *et al* 2011) and nonlinear indices (Porta *et al* 2011, Javorka *et al* 2011) have also been proposed to assess causality (Nollo *et al* 2009).

The main purpose of this paper is to present a methodology to characterize the dynamic interactions between RRV and SAPV, which includes the assessment of both the strength and the prevalent direction of local coupling. This methodology is based on the smoothed pseudo-Wigner–Ville distribution (SPWVD) and provides time–frequency (TF) representations of the signal power spectra, spectral coherence and phase differences with fine joint TF resolution. It also allows estimating the time course of the local coupling, phase differences and time-delay between the LF and HF spectral components of the two signals. Robust estimates of the BRS are obtained owing to the localization of TF regions characterized by statistically significant coherence and in which the SAPV leads the RRV signal.

The capability of reliably estimating fast changes in these dynamic interactions is assessed in a simulation study involving data recorded from healthy subjects.

A physiological study is carried out to characterize the cardiovascular dynamics during the head-up tilt table test (Freeman 2006, Mainardi *et al* 1997, Cooke *et al* 1999, Westerhof *et al* 2006, Porta *et al* 2011), and the Eurobavar data set (EDS) (Laude *et al* 2004, Westerhof *et al* 2004, Gouveia *et al* 2009) is analyzed to assess whether the presented methodology can be considered as the generalization of traditional time-invariant methods. To highlight the importance of non-stationary signal processing in the assessment of short-term cardiovascular control, a test of stationarity (Borgnat *et al* 2010) is applied to the signals analyzed in this paper.

2. Methods

2.1. Assessment of non-stationarity

Stationarity is usually assumed based on some arbitrary considerations. Recently, Borgnat *et al* (2010) proposed an operational framework for statistically testing stationarity relatively to an observation scale. The test is based on the comparison between global and local TF features. Stationarity occurs if the local spectra, evaluated at different time instants, are statistically similar to the global spectrum obtained by marginalization (details about how this test has been used are available at stacks.iop.org/PM/33/315/mmedia). The test was applied to the signals analyzed in this study.

2.2. TF representations

2.2.1. TF power spectra. Auto and cross TF spectra $S_{xy}(t, f)$ are estimated by the SPWVD, a member of the Cohen's class, characterized by the independent filtering in time and frequency. It is defined as (Hlawatsch and Boudreaux-Bartels 1992)

$$S_{xy}(t,f) = \iint\limits_{-\infty}^{+\infty} \Phi(\tau, \nu) A_{xy}(\tau, \nu) \, e^{j2\pi(t\nu - \tau f)} \, d\nu \, d\tau \tag{1}$$

$$A_{xy}(\tau, \nu) = \int_{-\infty}^{\infty} x\left(t + \frac{\tau}{2}\right) y^*\left(t - \frac{\tau}{2}\right) e^{-j2\pi \nu t} \, dt. \tag{2}$$

In these expressions, $A_{xy}(\tau, \nu)$ is the cross-ambiguity function. Separable smoothing is performed by an exponential kernel function, defined in the ambiguity function domain as $\Phi(\tau, \nu)$, and in the TF domain as $\phi(t, f)$:

$$\Phi(\tau, \nu) = \exp\left\{ -\pi \left[\left(\frac{\nu}{\nu_0}\right)^2 + \left(\frac{\tau}{\tau_0}\right)^2 \right]^{2\lambda} \right\}, \qquad \phi(t, f) = \iint\limits_{-\infty}^{+\infty} \Phi(\tau, \nu) \, e^{i2\pi(t\nu - \tau f)} \, d\tau \, d\nu. \tag{3}$$

The iso-contours of $\Phi(\tau, \nu)$ are the ellipses whose eccentricities depend on the parameters ν_0 and τ_0 (Costa and Boudreau-Bartels 1995). The parameters ν_0 and τ_0 are used to determine the degree of time and frequency filtering, respectively, while λ sets the roll-off of the kernel.

The resolution of the SPWVD is given by the shape of the kernel function. Time resolution is quantified by the full-width at half-maximum of $\phi(t, 0)$, i.e. (Δ_t), while frequency resolution is quantified by the full-width at half-maximum of $\phi(0, f)$, i.e. (Δ_f) (Orini *et al* 2011). These quantities measure the degree of spreading of a line in the TF domain: Δ_t and Δ_f are equal to the full-width at half-maximum of the SPWVD of a Dirac impulse, evaluated along t, and of a sinusoid, evaluated along f, whose ideal TF representations would be, in the absence of smoothing, straight lines.

2.2.2. TF coherence. TF coherence (TFC) measures the degree of local coupling between two signals and is given by (Matz and Hlawatsch 2000, White and Boashash 1990, Orini *et al* 2011)

$$\gamma(t, f) = \frac{|S_{xy}(t, f)|}{\sqrt{S_{xx}(t, f) S_{yy}(t, f)}}; \quad \gamma(t, f) \in [0, 1]. \tag{4}$$

Auto- and cross-spectra by the SPWVD are not always positive, and negative values are related to the presence of residual interference terms (Hlawatsch and Boudreaux-Bartels 1992). These terms may cause $\gamma(t, f)$ to take values outside the range [0,1], thus losing its physical interpretation. To obtain meaningful TFC estimates, the filtering provided by $\Phi(\tau, \nu)$ should completely suppress the interference terms (Matz and Hlawatsch 2000). The appropriate degree of TF smoothing is determined by fixing a desired TF resolution and by iteratively increasing the degree of smoothing by changing parameters τ_0 and ν_0, until reaching $\gamma(t, f) \in [0, 1]$. The results of this numerical process will be shown in section 4.

A statistical test is necessary to assess the coherence estimates, because, similar to stationary spectral coherence, TFC estimates depend on the parameters used in their calculation (Orini *et al* 2011). More specifically, the finer the TF resolution is, the higher should be the TFC estimates to be considered as statistically significant (Orini *et al* 2011). The TF regions where spectral coherence is significant are localized by a hypothesis test. The test is based on the comparison of $\gamma(t, f)$ with a threshold function $\gamma_{TH}(t, f)$ obtained as the 95th percentile of the statistical distribution $\Gamma(t, f) = \{\gamma_1(t, f), \ldots, \gamma_j(t, f), \ldots\}$, where $\gamma_j(t, f)$ is the TFC between the jth realization of two complex white Gaussian noises (Orini *et al* 2011). The region where $\gamma(t, f)$ is significant is defined in each band $B \in \{LF, HF\}$ as

$$\Omega_B \equiv \{(t, f) \in (\mathbb{R}^+ \times B) \mid \gamma(t, f) > \gamma_{TH}(t, f)\}. \tag{5}$$

2.2.3. TF phase-difference spectrum. The TF representation of the phase differences between the spectral components of two signals can be obtained by estimating the phase of $S_{xy}(t, f)$. The TF phase-difference (TFPD) spectrum is given by

$$\Theta(t, f) = \arctan\left[\frac{\Im[S_{xy}(t, f)]}{\Re[S_{xy}(t, f)]}\right], \qquad \Theta(t, f) \in [-\pi, \pi]. \tag{6}$$

Analytical expressions of the TFPD spectrum for linear chirps are available at stacks.iop.org/PM/33/315/mmedia.

2.3. Time course of the physiological indices

The time course of the indices characterizing the dynamic interactions between cardiovascular signals is estimated in specific TF regions. The localization of these regions is necessary to obtain robust and reliable estimates.

In the following paragraphs, the TF region from which the time course of a general index $\mathcal{I}_B(t) \in \{\gamma_B(t), \theta_B(t), \mathcal{D}_B(t), \alpha_B(t)\}$ is extracted is called $\Omega_B^{(\mathcal{I})}$, with $B \in \{$LF, HF$\}$.

2.3.1. Band coherence. The instantaneous frequencies of the spectral components of $|S_{xy}(t, f)|$, $f_B^{(xy)}(t)$, are estimated by localizing the corresponding instantaneous spectral peaks. Time-varying spectral bands centered around $f_B^{(xy)}(t)$ are defined as

$$\Omega_B^{(\gamma)} \equiv \left\{ (t, f) \in (\mathbb{R}^+ \times B) \mid f = f_B^{(xy)}(t) \pm \frac{\Delta_f}{2} \right\} \tag{7}$$

where Δ_f is a term related to the frequency resolution (see the previous section). The time course of the band coherence is then obtained by averaging $\gamma(t, f)$ in $\Omega_B^{(\gamma)}$:

$$\gamma_B(t) = \frac{1}{\Delta_f} \int_{\Omega_B^{(\gamma)}} \gamma(t, f) \, \mathrm{d}f. \tag{8}$$

2.3.2. Phase difference and time delay. The time course of the phase difference between each spectral component of the two signals, i.e. $\theta_B(t)$, is estimated in a TF region $\Omega_B^{(\theta)}$ centered around $f_B^{(xy)}(t)$ and where the coherence is statistically significant. These conditions are necessary because, in this context, the estimation of a phase difference is relevant only in time intervals in which the signals are approximately sharing the same instantaneous frequency. The region $\Omega_B^{(\theta)}$ is defined as

$$\Omega_B^{(\theta)} \equiv \left\{ \Omega_B^{(\gamma)} \cap \Omega_B \right\} \circ R(t, f) \tag{9}$$

where $R(t, f)$ is a rectangle of sides $2s \times \frac{\Delta_f}{2}$ Hz and $\circ$ denotes the opening (processing technique that involves erosion and dilation). The opening excludes from $\{\Omega_B^{(\gamma)} \cap \Omega_B\}$ the portions of the TF domain, which are smaller than $R(t, f)$, thus adding robustness to the final estimates. The indices $\theta_B(t)$ and $\mathcal{D}_B(t)$ are estimated (in radians and seconds, respectively) as

$$\theta_B(t) = \left[\int_{\Omega_B^{(\theta)}} \Theta(t, f) \, \mathrm{d}f \right] \Big/ \left[\int_{\Omega_B^{(\theta)}} \mathrm{d}f \right], \qquad \mathcal{D}_B(t) = \frac{\theta_B(t)}{2\pi f_B^{(xy)}(t)}. \tag{10}$$

Analytical expressions for indices $\theta_B(t)$ and $\mathcal{D}_B(t)$ for linear chirps are available at stacks.iop.org/PM/33/315/mmedia.

2.3.3. Baroreflex sensitivity. The index $\alpha_B(t)$, which measures the changes in the spontaneous BRS, is estimated in a TF region $\Omega_B^{(\alpha)}$ centered around $f_B^{(xy)}(t)$, where coherence is statistically significant and where a change in the SAPV signal precedes a correlated change in the RRV signal:

$$\Omega_B^{(\alpha)} = \left\{ (t, f) \in \Omega_B^{(\theta)} \mid \Theta(t, f) < 0 \right\}. \tag{11}$$

According to the described framework, if we associate $x(t)$ and $y(t)$ with the RRV and SAPV signals, respectively, when a change in the arterial pressure precedes a corresponding change in the heart period, the phase of $S_{xy}(t, f)$ is negative, i.e. $\Theta(t, f) < 0$ (see expressions available at stacks.iop.org/PM/33/315/mmedia). The time course of the BRS is then estimated as

$$\alpha_B(t) = \sqrt{\int_{\Omega_B^{(\alpha)}} S_{xx}(t, f) \, \mathrm{d}f \Big/ \int_{\Omega_B^{(\alpha)}} S_{yy}(t, f) \, \mathrm{d}f}. \tag{12}$$

3. Material and study populations

The presented methodology was assessed in a simulation study and was used to analyze cardiovascular interactions in two different data sets.

3.1. Simulation study

A simulation study was carried out with the purpose of validating the proposed methodology. The signals used in these simulations were the modified versions of the RRV signals recorded during the tilt table test described in the following section. They were obtained as

$$x(t) = a_{RRV}(t) + w_x(t), \qquad y(t) = [\gamma_0(t)\alpha_0(t)\exp(j\theta_0(t))]a_{RRV}(t) + w_y(t) \tag{13}$$

where $a_{RRV}(t)$ is the complex analytic signal representation of the RRV signal, and $w_x(t)$ and $w_y(t)$ are the white Gaussian noises associated with SNR = 10 dB. The indices $\gamma_0(t) \in \{0, 1\}$, $\theta_0(t) \in [-2.2, -0.8]$ rad and $\alpha_0(t) \in [5, 20]$ ms mmHg^{-1} represent the reference time course of the local coupling, phase difference, and BRS (time courses are shown in figure 3). The reasons that make the estimation of these indices challenging are as follows. The TF structure of the signals reflects the complexity of real non-stationary biomedical signals; the presence of epochs, the shortest lasting for 30 s, during which signals are not locally coupled and during which $\theta_B(t)$ and $\alpha_B(t)$ should not be estimated; the phase difference varies nonlinearly with time; the BRS first undergoes stepwise changes and then recovery toward higher values following a nonlinear timecourse; the noise is added; and finally, all these patterns imply simultaneous amplitude and frequency modulation of the signals.

3.2. Tilt table test analysis

Fourteen subjects (aged 29 $\pm$ 3 years) underwent a tilt table test with the following protocol: 4 min in early supine position (T_{es}), 5 min head-up tilted to an angle of 70° (T_{ht}), and 4 min back to later supine position (T_{ls}) (Mincholé *et al* 2011). The automatic bed took about 18 s to move from 0° to 70°. The ECG signals were recorded using the BIOPAC MP 150 system with a sampling frequency of 1 kHz. The temporal location of the nth QRS complex in the ECG, i.e. t_n^{QRS}, was automatically determined using the algorithm described by Martinez *et al* (2004). The RR series was estimated as $x_{RR}(n) = t_{n+1}^{QRS} - t_n^{QRS}$, and the value $x_{RR}(n)$ was associated with the time instant t_n^{QRS}. The effect of abnormal RR intervals was corrected by applying a methodology described by Mateo and Laguna (2003). The pressure signal was recorded at the finger by the Finometer system with a sampling frequency of 250 Hz and without correction for the hydrostatic gradient change during tilt. The systolic arterial pressure series was obtained as the maximum of the pressure signal within a short interval following t_n^{QRS}. During the procedure, the Finometer was recalibrated at the beginning of T_{ht} and T_{ls}. The recalibration took a few seconds and introduced artifacts that were corrected by interpolation. The time series were subsequently interpolated by a fifth-order spline with a sampling frequency of 4 Hz, and the RRV and SAPV signals, namely $x_{RRV}(t)$ and $x_{SAPV}(t)$, were obtained by high-pass filtering with a cut-off frequency of 0.03 Hz.

3.3. Eurobavar study

The experimental setting is described in detail by Laude *et al* (2004). Briefly, 21 subjects (aged 38.4 $\pm$ 3.3 years) were included in the study. The subjects were comprised of 4 healthy volunteers, 12 normotensive outpatients, 3 hypertensive patients (1 untreated), 1 diabetic patient with cardiac autonomic neuropathy (DAN), and 1 subject who recently underwent heart
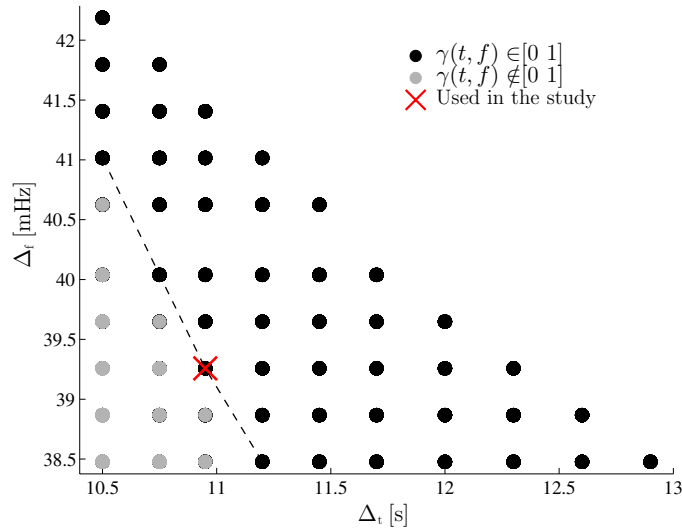
Figure 1. Circles represent the TF resolution obtained by tuning the parameters of the kernel in (3). The kernels that gave $\gamma(t, f) \in [0, 1]$ for the entire data set described in section 3.2 are indicated in black, and those that gave $\gamma(t, f) \notin [0, 1]$ for at least one subject are denoted in gray. The cross represents the resolution of the kernel used in this study.

transplantation (HTR). ECG and pressure signals were acquired with a sampling frequency of 500 Hz in supine and standing positions (about 10 min, respectively).

4. Results

Although the SPWVD gives the possibility of using an independent filtering in time and frequency, the constraint of having $\gamma(t, f)$ bounded between 0 and 1 imposes a sort of trade-off between time and frequency resolutions, which cannot be simultaneously and arbitrarily fine. For a given set of signals, different combinations of time and frequency resolutions fulfill the condition $\gamma(t, f) \in [0, 1]$. In figure 1, black circles represent the available choices of TF resolutions offered by the kernel in (3) that, for the whole data set described in section 3.2, gave $\gamma(t, f) \in [0, 1]$; gray circles represent the TF resolutions that led to $\gamma(t, f) \notin [0, 1]$ for at least one subject. The closer a point is to the origin of the axes, the finer is the TF resolution. Thus, the most interesting combinations of TF resolutions are those indicated with the dashed line. In the following, the kernel $\Phi(\tau, \nu)$ that gave $\{\Delta_t, \Delta_f\} = \{10.95 \text{ s}, 39.2 \text{ mHz}\}$ was used (see the cross mark in figure 1).

4.1. Assessment of non-stationarity

In both the data sets, the hypothesis of stationarity was assessed via the statistical framework described, available at stacks.iop.org/PM/33/315/mmedia (Borgnat *et al* 2010). Figure 2 shows, for a given scale of observation, the relative number of signals that were considered non-stationary by the test. The scale of observation is given as $T_h/T \in [0.05, 0.5]$, where T_h is the length of the window of the spectrogram and T is the length of the signals. Depending on the signal, T_h varies from 30–40 s to 5–7 min.
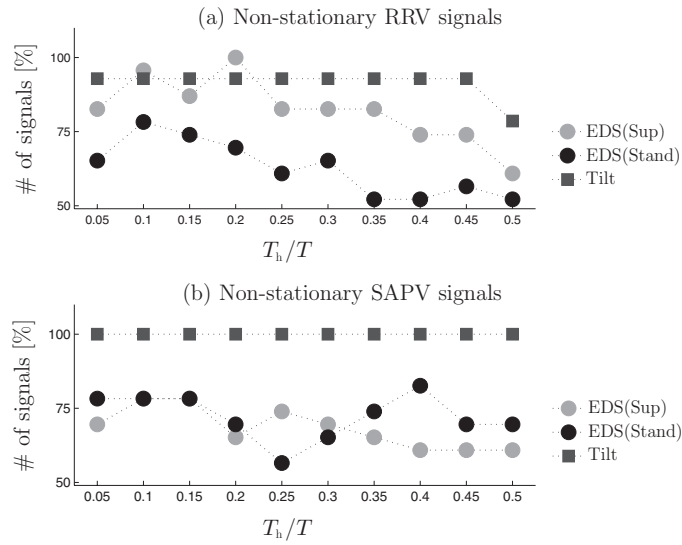
Figure 2. Outcomes of the non-stationary test. Results are given as the number of signals that were considered non-stationary. Signals recorded during the tilt table test are denoted by square marks. Signals from the EDS recorded in supine and standing position are represented by gray and black circles, respectively.

All the SAPV signals recorded during the tilt table test were considered non-stationary at every time scale, while 1 over 14 RRV signals was considered, for each T_h/T, stationary. Interestingly, more than 50% of the signals from the EDS were considered non-stationary, despite the fact that they were recorded in resting conditions. In figure 2(a), it is shown that for $x_{RRV}(t)$, the typical scale of non-stationarity (Borgnat *et al* 2010), at which it is more likely to reject the null hypothesis of stationarity, corresponds to $T_h/T = 0.1$–0.2 (about 1–2 min). In addition, it is also shown that the number of non-stationary RRV signals was higher in supine than in the standing position. In the supine position, for $T_h/T < 0.4$, the non-stationary testing was positive for more than 80% of the signals, and for $T_h/T = 0.2$, stationarity was rejected in all the signals. In figure 2(b), it is shown that at about the same scale of observation, about 80% of the SAPV signals were considered non-stationary, regardless of the position of the subjects.

4.2. Simulation study

In the simulation study, from each of the 14 RRV signals, 50 couples of modified signals were generated. For every couple of signals, the general index $\mathcal{I}(t) \in \{\gamma(t), \theta(t), \alpha(t)\}$ was estimated in the TF regions $\Omega_B^{(\mathcal{I})}$, and the time course was $\mathcal{I}(t) = (\mathcal{I}_{LF}(t) + \mathcal{I}_{HF}(t))/2$. The results are shown in figure 3. Figure 3(a) depicts the results of coherence analysis. The mean threshold $\overline{\gamma_{TH}} \approx 0.85$ is reported by a dashed line. Epochs of decorrelation and correlation were localized with a high temporal resolution. As shown in this illustration, the difference $t_0 - \hat{t}_0$ between the occurrence of an abrupt change of $\gamma_0(t)$ and the time instant at which the median time course of $\gamma(t)$ matches the threshold value ($\gamma^m(\hat{t}_0) = \overline{\gamma_{TH}}$) was 0, 1.5, and 2.25 s, respectively. It can be noted that the minimum level of coherence was higher than 0 due to the effect of the kernel, while the maximum level of coherence was lower than 1 due to the effect of the phase differences and due to the noise. The decrease in $\gamma(t)$ observed at around
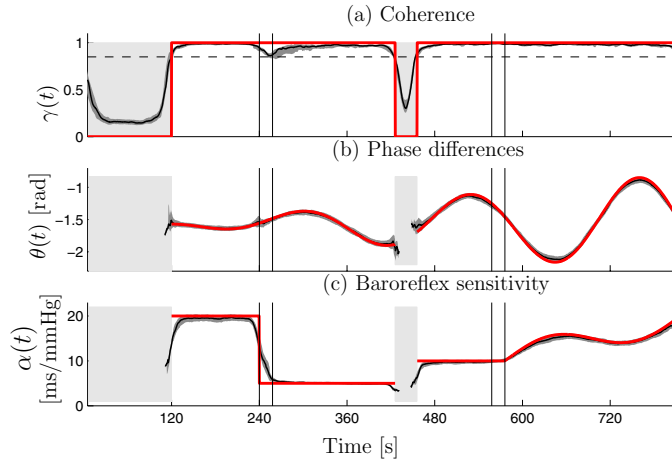
Figure 3. Simulation: time course of (a) coherence, (b) phase differences, and (c) BRS. The reference values $\gamma_0(t)$, $\theta_0(t)$, and $\alpha_0(t)$ are represented by bold thick/red lines. Estimates are represented as median (black line) and interquartile range (black lines). Vertical lines mark supine positions and head-up tilt. Light gray areas represent the intervals during which signals are uncoupled.

$t = 240$ s was due to the stepwise decrease in $\alpha_0(t)$ (see figure 3(c)). Figure 3(b) shows that the phase-difference estimator (10) gave an accurate tracking of the time course of $\theta_0(t)$. As $\Omega_B^{(\theta)}$ includes only regions where $\gamma(t, f)$ is significant, estimates were given only in TF regions where the signals were locally coupled. In figure 3(c), it is shown that the time course of $\alpha(t)$ was estimated with high accuracy. The stepwise decrease in $\alpha(t)$ from 20 to 5 ms mmHg^{-1} was approximated by a sigmoid-like pattern. Again, the coherence analysis prevented from including the interval where signals were uncoupled in the analysis.
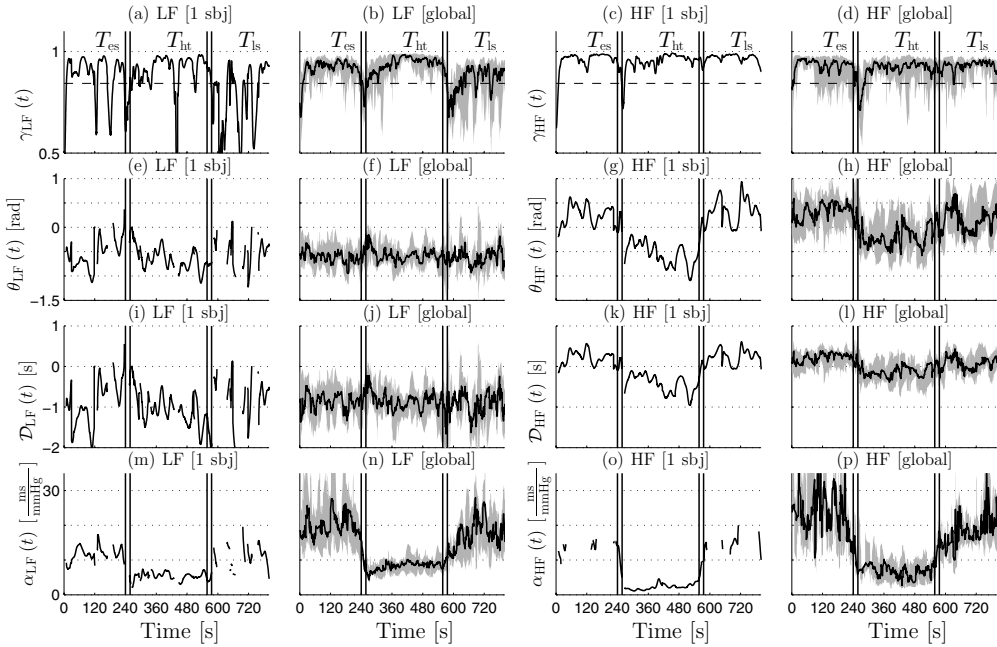
4.3. Tilt table test

The TF representations obtained from the analysis of RRV and SAPV of one subject (male, 30 years old) are shown in figure 4. In the auto-spectra, shown in figures 4(a) and (b), the power of the HF modulation was higher than that of the LF one. During the head-up tilt, the powers of $x_{\mathrm{RRV}}(t)$ and $x_{\mathrm{SAPV}}(t)$ decreased and increased, respectively. The instantaneous frequencies of the HF component of both the signals, as well as those of the cross-spectrum (see $\Omega_B^{(\gamma)}$ in figure 4(c)), reflect the high variability of the respiratory rate, which fluctuated between 0.15 and 0.25 Hz. Despite the non-stationary structure of the signals, the regions in which the local coupling was statistically significant were localized by the TFC analysis (see figure 4(c)). The head-up tilt caused the TFPD spectrum $\Theta(t, f)$, shown in Fig 4(d), to change quickly, especially in the HF range. In figures 4(c) and (d), the regions $\Omega_B^{(\gamma)}$ and $\Omega_B^{(\theta)}$ are encircled by white contours. By averaging in traditional spectral ranges, instead of using these specific regions, one would have estimated a much lower coherence in the HF range and erroneously detected abrupt changes of phase difference in correspondence with those TF regions in which the signals were not locally coupled (as in the LF at $t \approx 240$ s and $t \approx 600$ s).

The time course of the physiological indices derived from the spectra of figure 4, as well as the global results, is shown in figure 5, while the numerical results are given in table 1. In the calculation of these values, the first and last $2\Delta_t$ have been excluded
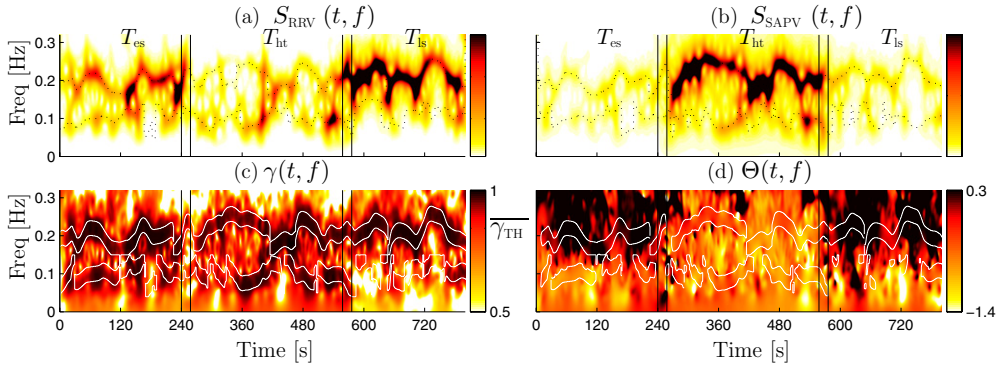
Figure 4. TF representation from one subject: (a), (b) SPWVD of $x_{RRV}(t)$ and $x_{SAPV}(t)$, respectively, and instantaneous frequencies are represented by a dotted line; (c) TF coherence $\gamma(t, f)$; and (d) TF phase-difference spectrum $\Theta(t, f)$. In (c) and (d), $\Omega_B^{(\gamma)}$ and $\Omega_B^{(\theta)}$ are encircled by a white contour. The vertical lines denote supine positions and head-up tilt.

Figure 5. Indices during the tilt table test: (a)–(d) local coupling $\gamma_B(t)$ as in (8); (e)–(h) phase differences $\theta_B(t)$ as in (10); (i)–(l) time delay $\mathcal{D}_B(t)$ as in (10); and (m)–(p) BRS $\alpha_B(t)$ as in (12). First and third columns: results from the subject whose TF representations are shown in figure 4. Second and fourth columns: global results shown as median (black lines) and interquartile range (shadowed areas) of the time courses from all the subjects. The vertical lines denote supine positions and head-up tilt.

from each of the three epochs. The Wilcoxon rank sum test was applied to statistically compare the temporal mean values of the indices estimated in each of the three conditions, i.e. $\{\overline{\mathcal{I}_{B,1}(t \in T_k)}, \dots, \overline{\mathcal{I}_{B,L}(t \in T_k)}\}$ and $\{\overline{\mathcal{I}_{B,1}(t \in T_l)}, \dots, \overline{\mathcal{I}_{B,L}(t \in T_l)}\}$, where $T_k \neq T_l \in$

Table 1. Global results of the tilt table test, reported as the average of the median trends shown in figure 5, evaluated in epochs T_{es}, T_{ht}, and T_{ls} (first and last $2\Delta_t$ have been excluded from the analysis). '†' denotes that the mean values of a given index are statistically significant with respect to those estimated during the head-up tilt T_{ht} ($P < 0.05$).

Index	Ω_{LF}			Ω_{HF}		
	T_{es}	T_{ht}	T_{ls}	T_{es}	T_{ht}	T_{ls}
$\overline{\gamma_B(t)}$ (n.u.)	0.93 ± 0.02	0.95 ± 0.04	$0.89 \pm 0.08^{\dagger}$	0.95 ± 0.02	0.93 ± 0.03	0.94 ± 0.01
$\overline{\theta_B(t)}$ (rad)	-0.59 ± 0.16	-0.59 ± 0.15	-0.61 ± 0.23	$0.37 \pm 0.23^{\dagger}$	-0.27 ± 0.22	0.14 ± 0.38
$\overline{\mathcal{D}_B(t)}$ (s)	-0.85 ± 0.29	-0.86 ± 0.22	-0.84 ± 0.40	$0.26 \pm 0.14^{\dagger}$	-0.16 ± 0.16	0.08 ± 0.24
$\overline{\alpha_B(t)}$ (ms mmHg^{-1})	$19.77 \pm 4.51^{\dagger}$	8.62 ± 1.21	$17.87 \pm 4.44^{\dagger}$	$23.72 \pm 7.66^{\dagger}$	6.92 ± 2.51	$18.24 \pm 4.09^{\dagger}$

$\{T_{es}, T_{ht}, T_{ls}\}$ is the index of the epochs and $L \leqslant 14$ are the subjects (subjects for which $\mathcal{I}(t)$ was not estimated for more than half the duration of the tilt table test were excluded from the statistical analysis).

In figure 5(b), it is shown that during the position changes, $T_{es} \to T_{ht}$ and $T_{ht} \to T_{ls}$, the time course of $\gamma_{LF}(t)$ is characterized by two patterns, a first abrupt decrease and a subsequently slower increase. During the head-up tilt, restoration of baseline values took about 2 min, and about 1 min later, the median $\gamma_{LF}(t)$ reached values as high as 0.99. After coming back to the supine position, $\gamma_{LF}(t)$ maintained lower values than during the early supine position. In HF, $\gamma_{HF}(t)$ fluctuated around 0.93 ± 0.02 and did not decrease during the position change from $T_{ht} \to T_{ls}$. In the LF range, the phase differences $\theta_{LF}(t)$ were about -0.60 ± 0.11 rad ($\mathcal{D}_{LF}$ were about 875 ± 190 ms), thus revealing that a change in the LF oscillation of $x_{SAPV}(t)$ preceded a correlated change in the LF oscillation of $x_{RRV}(t)$. In the HF range, the head-up tilt provoked a decrease in $\theta_{HF}(t)$ from positive to negative values, thus showing a change in the prevalent direction of the local coupling between the respiratory-related oscillations of $x_{SAPV}(t)$ and $x_{RRV}(t)$. The index $\alpha_B(t)$ was estimated only in the regions centered around $f_B^{(xy)}(t)$, where the local coupling was significant and the phase difference was negative. These conditions determined, for the subject whose TF representations are shown in figure 4, the patterns observed in figures 5(m) and (o). Globally, as shown in figures 5(n) and (p), $\alpha_B(t)$ decreases from about 20 ms mmHg^{-1} during T_{es} and T_{ls}, to less than 9 ms mmHg^{-1} during T_{ht}. Interestingly, the decrease in both $\alpha_{LF}(t)$ and $\alpha_{HF}(t)$ due to the head-up tilt took a few seconds, while the following increase due to coming back later to the supine position was remarkably slower.

4.4. Eurobavar data set

To assess whether the presented framework can be considered as a generalization of traditional analysis, the EDS was processed by both stationary framework (SF) and non-stationary framework (NS), and the results were compared to those presented by Laude *et al* (2004). In the SF, indices were obtained by temporal averaging of the TF distributions described in section 2.2, thus representing stationary analysis (marginal spectra were used to obtain power and coherence estimates). In the NF, for every subject, the temporal mean of the non-stationary indices described in section 2.3 was estimated. The results of the NF and SF are illustrated in the graphics on the left and right sides of figure 6, respectively. In figures 6(a)–(d), circles and bars represent the mean and the standard deviation of local coupling and phase differences of the subjects without baroreflex impairment, while in figures 6(e)–(f), circles and bars represent the mean and the standard error of the BRS for the same subjects. (The standard error was
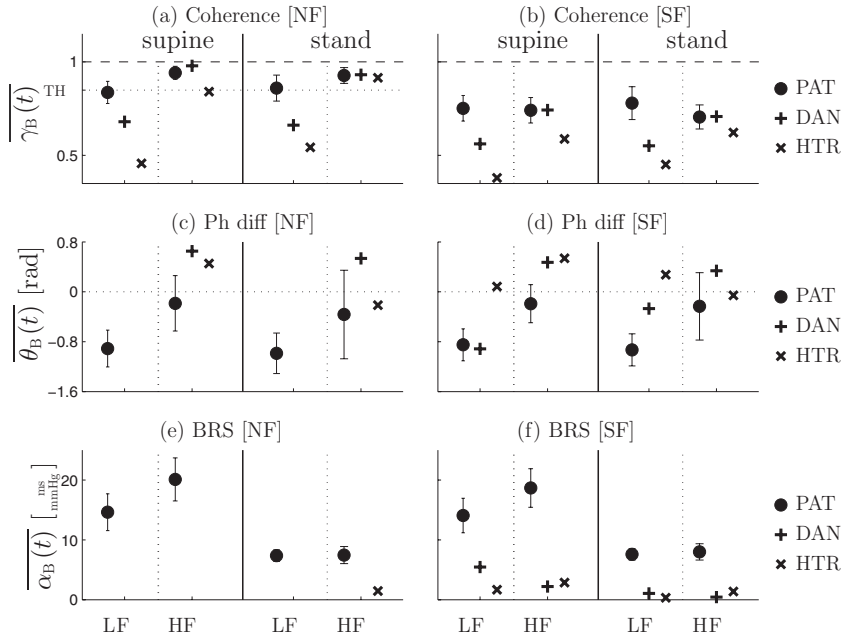
Figure 6. Eurobavar data set. (*Left*) The results obtained by the presented NF. (*Right*) The results obtained by the SF, as defined in section 2.2. Markers $+$ and $\times$ represent diabetic patient with cardiac autonomic neuropathy (DAN) and HTR, respectively. Circles represent the rest of patients (PAT). (a), (b) The mean $\pm$ standard deviation of coherence across subjects. (c), (d) The mean $\pm$ standard deviation of phase difference across subjects. (e), (f) The mean $\pm$ standard error of BRS across subjects. Note that in the NF, phase differences were estimated only for subjects for which coherence estimates were significant for more than 95% of the total length of the recording, while BRS was reported only if phase-difference estimates were negative.

estimated for comparison with that of Laude *et al* (2004).) In these graphics, markers $+$ and $\times$ represent the DAN and the HTR patient, respectively. The presented methodology (NF) gave higher coherence estimates than the SF. Moreover, coherence estimates obtained by the NF were higher in the HF than in the LF. These differences were due to the use of $\Omega_{\mathrm{B}}^{(\gamma)}$. In $\Omega_{\mathrm{LF}}^{(\gamma)}$, the coupling of the signals from the HTR and DAN patients was not significant for more than 95% of the total length of the recording. Because of the absence of local coupling, in HTR and DAN, the phase differences $\theta_{\mathrm{LF}}(t)$ and BRS $\alpha_{\mathrm{LF}}(t)$ were not assessed. Without performing the statistical analysis on the coherence estimates, one could erroneously conclude that in the HTR patient, $\overline{\theta_{\mathrm{LF}}(t)} > 0$. For subjects without baroreflex impairment, estimates of the BRS obtained by both SF and NF were consistent with those obtained by traditional time-invariant methodologies (Laude *et al* 2004, Westerhof *et al* 2004). In the SF, for subject without baroreflex impairment (see figure 6(f)), $\overline{\alpha_{\mathrm{LF}}(t)}$ was 14.07 ± 2.88 ms mmHg^{-1} (supine) and 7.58 ± 0.96 (standing) ms mmHg^{-1}, while $\overline{\alpha_{\mathrm{HF}}(t)}$ was 18.66 ± 3.23 ms mmHg^{-1} (supine) and 8.00 ± 1.36 ms mmHg^{-1} (standing). The supine to standing ratio was 1.86 and 2.33 in LF and HF ranges, respectively, which is in line with that obtained in Laude *et al* (2004). By using the presented framework, evidences of the baroreflex impairment of DAN and HTR patients were given by high $\theta_{\mathrm{HF}}(t)$, by the persistent absence of coupling between the signals in LF, and highlighted by the fact that no $\alpha(t)$ index could be estimated.

5. Discussion

5.1. The cross TF framework

The main purpose of the presented framework is to propose a methodology for the characterization of the dynamic interactions between RRV and SAPV, which accounts for the intrinsic non-stationarity of the cardiovascular system, and which includes the assessment of both the strength and the prevalent direction of the coupling. The analysis is composed of the following steps. (i) Choice of the parameters of the kernel of type (3) for the estimation of the SPWVD. Among those kernels that can be used in coherence analysis, the one that gives the more appropriate TF resolution should be used (see figure 1). (ii) Estimation of the TF power, coherence, and phase-difference spectra. (iii) Localization of specific TF regions from which the indices that describe the cardiovascular interactions are extracted. (iv) Estimation of indices that quantify the strength of the local coupling $\gamma_B(t)$, the degree of synchronization $\theta_B(t)$, the latencies $\mathcal{D}_B(t)$, and the BRS $\alpha_B(t)$.

The advantage of the SPWVD over other TF distributions, such as wavelet and spectrogram, is that it offers the possibility of determining the shape of the smoothing function both in time and frequency, which in turn allows for more accurate localization of cardiovascular dynamics (Orini *et al* 2011). The quantification of the TF resolution of the SPWVD by Δ_t and Δ_f, which is crucial to correctly interpret the results, can also be used to compare the resolution of the SPWVD with that of other types of distributions.

The analysis of the phase differences between $x_{RRV}(t)$ and $x_{SAPV}(t)$ is used to infer the prevalent direction of the coupling and the time delay, which characterize the system. This is necessary to accept the hypothesis of the involvement of the baroreflex in the observed changes. Such a sensitive issue requires robust and accurate estimates. In our framework, robustness and accuracy are ensured by the fact that phase differences are estimated only in TF regions where the local coupling is statistically significant. These regions have a relatively small frequency width Δ_f, and a further control over their size is done by the opening.

Despite the great number of methodologies proposed for the assessment of the baroreflex, only a few combine non-stationary processing, statistical coherence analysis and assessment of the prevalent causal direction of local coupling. In this methodology, the interactions between the TF structure of the signals are characterized without imposing any assumption or model to the signals. Furthermore, neither coefficient identification nor parameter initialization is needed. Although the linear synchronization indices used in this framework give a rather basic description of the interaction between complex systems (Xiao *et al* 2005), they have a clear physical interpretation: $\gamma(t, f)$ quantifies the strength of the local coupling, thus allowing to localize TF regions where signals share approximately the same instantaneous frequency, while $\Theta(t, f)$ quantifies the phase differences, thus allowing to estimate the time delays between changes in the spectral components of two signals and determine, in specific TF regions, which signal is leading which.

The SPWVD, whose main property is the independent TF filtering giving high resolution, has never been used to estimate the BRS as well as the phase differences between cardiovascular signals. Recently, other methods for the estimation of phase differences in the joint TF domain, based on Rihaczek (Aviyente *et al* 2010), wavelet (Cnockaert *et al* 2008, Lachaux *et al* 2002) and reduced interference (Shin *et al* 2005) transforms, have been proposed. Contrary to synchronization indices based on the Hilbert transform (Ocon *et al* 2011), the presented methodology offers the possibility of separately assessing the degree of synchronization between LF and HF spectral components. Concerning the estimation of TF coherence by the SPWVD, the most important issue is the definition of a kernel that completely suppresses

the interference terms inherent to the Wigner–Ville distribution. A sufficient smoothing would ensure both positivity of the spectra and boundness of the TF coherence (Matz and Hlawatsch 2000). Kernels of type (3) have been shown to provide such a smoothing and have been recently used in the cross TF analysis of cardiovascular signals (Gil *et al* 2010, Orini *et al* 2011).

The results of the simulation study show that this framework is robust and accurate.

To provide a more comprehensive characterization of the cardiovascular interactions, other important physiological parameters, such as respiration, may be included in further studies.

5.2. Response to the head-up tilt

Mechanisms regulating the cardiovascular response to a passive head-up tilt are predominantly studied (Freeman 2006, Mainardi *et al* 1997, Cooke *et al* 1999, Nollo *et al* 2005, Westerhof *et al* 2006, Porta *et al* 2011, Ocon *et al* 2011). Our results show that the local coupling between RRV and SAPV is statistically significant both in the LF and HF during most part of the test, even at rest in the supine position. During the position changes, the level of coherence abruptly decreased. The time taken by the signals to resynchronize, i.e. to restore significant level of coherence, characterizes the temporal pattern of response of the short-term cardiovascular regulation to an external perturbation.

The results shown that in the LF range, SAPV led RRV during the entire test. In the HF range, SAPV led RRV only during the head-up tilt. These results are in line with those observed in other studies (Cooke *et al* 1999, Nollo *et al* 2005, Porta *et al* 2011). Owing to the periodicity of the phase differences, it may be possible that instead of the fact that in the LF range, $x_{SAPV}(t)$ was leading $x_{RRV}(t)$ with $|\theta_{LF}(t)| \approx 0.6$ rad, $x_{RRV}(t)$ was actually leading $x_{SAPV}(t)$ with $|\theta_{LF}(t)| \approx 5.7$ rad. However, this last possibility, which would imply, for $f_{LF} = 0.09$ Hz, a time delay of about 10 s, is unlikely, not only because it largely exceeds the range of baroreflex latency ([0.24, 3] s) (Cooke *et al* 1999), but also because in this NF, such a time delay (close to Δ_t) would not be consistent with the level of local coupling as high as $\gamma_{LF}(t) \approx 0.99$.

The time course of the BRS $\alpha_B(t)$ followed similar patterns both in $\Omega_{LF}^{(\alpha)}$ and $\Omega_{HF}^{(\alpha)}$ ranges. In the supine position, the high variability of $\alpha_{HF}(t)$ was due to the fact that it was estimated in a few subjects, because in most of them $\theta_{HF}(t) > 0$. As expected, the BRS was higher during the supine position and lower during the head-up tilt. During the position changes, the index $\alpha_B(t)$ was characterized by two different dynamics: when subjects were passively moved from the supine to the standing position, $\alpha_B(t)$ decreased in a few seconds, while when subjects were moved from the standing to the supine position, $\alpha_B(t)$ increased gradually.

5.3. Eurobavar data set

The study of the EDS showed that (i) non-stationary signal processing should be preferred to study the biomedical signals even when they are acquired in conditions that are usually assumed as stationary and (ii) the proposed framework can be considered as an improved TF generalization of traditional spectral methods of analysis.

It is widely accepted that biomedical signals are intrinsically non-stationary. The outcomes of the test proposed by Borgnat *et al* (2010) confirm that the hypothesis of stationarity is often rejected even for signals recorded during rest. Moreover, it was shown that signals were more likely considered non-stationary for a temporal scale of observation of about 1–2 min.

To compare the results provided by the presented methodology with those obtained by traditional time-invariant ones, we used the results obtained by marginalizing the TF

representations given by the SPWVD as reference. The results given by this SF are within the variability of those obtained with different techniques of the time-invariant analysis (Laude *et al* 2004). Although the mean results obtained by the presented NF are different, they are in line with those obtained by the SF and with those observed by Laude *et al* (2004). Our results show that in the diabetic subject with neuropathy and in the short-term transplanted patient, the baroreflex is not active. This implies a lack of coupling in the LF range and a causal direction from RRV to SAPV in the HF range. These results are in agreement with those observed by Porta *et al* (2011) and show that the presented methodology correctly detects impairments of the baroreflex.

5.4. Further considerations on the cross TF analysis of cardiovascular signals

In the cross TF analysis, the processing that leads to the estimation of the RRV and SAPV signals, $x_{\mathrm{RRV}}(t)$ and $x_{\mathrm{SAPV}}(t)$, is of crucial importance because it affects the estimation of the phase differences and latencies between them. For instance, it is worth noting that the results obtained by analyzing the RRV and SAPV cannot be directly extended to the interactions between the heart-rate variability and SAPV signals, because the phase differences between $x(t)$ and $y(t)$ are not equal to those between $x(t)$ and $1/y(t)$.

Furthermore, in the estimation of the RRV signal, three issues should be carefully taken into account. (i) The choice of the representations of the RRV signal, which can be based on the interpolation of the RR intervals, as done in this study, or on some other model (Sörnmo and Laguna 2005, Mateo and Laguna 2003, Chen *et al* 2011). (ii) The arbitrary assignation of a given heart period interval to a given temporal instant. The physiological phenomena that determine the duration of $t_{n+1}^{\mathrm{QRS}} - t_n^{\mathrm{QRS}}$ do not occur at time t_n^{QRS} neither at t_{n+1}^{QRS}, but they may be seen as continuous phenomena that are characterized based on information sampled at t_n^{QRS} and t_{n+1}^{QRS}. In this study, we used a non-causal representation of the heart period, i.e. we associated $(t_{n+1}^{\mathrm{QRS}} - t_n^{\mathrm{QRS}})$ with t_n^{QRS}. If we had used a causal representation of the heart period (Sörnmo and Laguna 2005), we would have obtained more negative phase differences between the spectral components of the signals, which in T_{es} and T_{ls} of the tilt table test may have allowed the estimation of $\alpha_{\mathrm{HF}}(t)$ for more subjects and longer intervals.

The estimation of the SAPV signal can also affect its degree of synchronization with the RRV signal. The main issue is the place where the arterial pressure is measured and the inclusion of the pulse transit time (PTT) in the estimation of the latencies (Gil *et al* 2010). Even in the ideal case in which changes in the SAPV and RRV are simultaneous, if the arterial pressure is measured at the finger and RR in correspondence with the heart beat, we would observe a delay related to the PTT.

These technical issues, which neither affect the relative changes of the indices nor the power estimates or the measures derived from them, should be carefully taken into account in the physiological interpretation of the phase differences and latencies.

6. Conclusions

In this paper, we present a TF framework to assess the dynamic interactions between RRV and SAPV, which accounts for the intrinsic non-stationarity of the cardiovascular system and includes the assessment of both the strength and the prevalent direction of local coupling. The cross TF analysis is appropriate since, as shown in this paper, cardiovascular signals are often non-stationary, coherence between them is intermittent and the direction of the coupling is not always consistent with the involvement of the baroreflex. Time-varying indices of coherence, phase difference and BRS were used to track changes provoked by the head-up tilt with fine

resolution, and they could be used to identify subjects with previously documented baroreflex impairment.

Most of the algorithms described in this paper can be freely downloaded at: http://www.micheleorini.com/.

The test of stationarity can be freely downloaded at: http://perso.ens-lyon.fr/patrick.flandrin/stat_test.html

Acknowledgments

References

Aviyente S, Bernat E M, Evans W S and Sponheim S R 2010 A phase synchrony measure for quantifying dynamic functional integration in the brain *Hum. Brain Mapp.* **32** 80–93

Barbieri R, Parati G and Saul J 2001 Closed- versus open-loop assessment of heart rate baroreflex *IEEE Eng. Med. Biol. Mag.* **20** 33–42

Borgnat P, Flandrin P, Honeine P, Richard C and Xiao J 2010 Testing stationarity with surrogates: a time–frequency approach *IEEE Trans. Signal Process.* **58** 3459–70

Chen Z, Purdon P L, Harrell G, Pierce E T, Walsh J, Brown E N and Barbieri R 2011 Dynamic assessment of baroreflex control of heart rate during induction of propofol anesthesia using a point process method *Ann. Biomed. Eng.* **39** 260–76

Cnockaert L, Migeotte P F, Daubigny L, Prisk G K, Grenez F and Sá R C 2008 A method for the analysis of respiratory sinus arrhythmia using continuous wavelet transforms *IEEE Trans. Biomed. Eng.* **55** 1640–2

Cooke W H, Hoag J B, Crossman A A, Kuusela T A, Tahvanainen K U O and Eckberg D L 1999 Human responses to upright tilt: a window on central autonomic integration *J. Physiol.* **517** 617–28

Costa A and Boudreau-Bartels G 1995 Design of time–frequency representations using a multiform, tiltable exponential kernel *IEEE Trans. Signal Process.* **43** 2283–301

de Souza Neto E P, Abry P, Loiseau P, Cejka J C, Custaud M A, Frutoso J, Gharib C and Flandrin P 2007 Empirical mode decomposition to assess cardiovascular autonomic control in rats *Fundam. Clin. Pharmacol.* **21** 481–96

Di Rienzo M, Parati G, Radaelli A and Castiglioni P 2009 Baroreflex contribution to blood pressure and heart rate oscillations: time scales, time-variant characteristics and nonlinearities *Phil. Trans. R. Soc.* A **367** 1301–18

Freeman R 2006 Assessment of cardiovascular autonomic function *Clin. Neurophysiol.* **117** 716–30

Gallet C, Chapuis B, Barres C and Julien C 2011 Time–frequency analysis of the baroreflex control of renal sympathetic nerve activity in the rat *J. Neurosci. Methods* **198** 336–43

Gil E, Orini M, Bailón R, Vergara J M, Mainardi L and Laguna P 2010 PTT variability for discrimination of sleep apnea related decreases in the amplitude fluctuations of PPG signal in children *Physiol. Meas.* **31** 1271

Gouveia S, Rocha A P, Laguna P and Lago P 2009 Time domain baroreflex sensitivity assessment by joint analysis of spontaneous SBP and RR series *Biomed. Signal Process. Control* **4** 254–61

Hlawatsch F and Boudreaux-Bartels G F 1992 Linear and quadratic time–frequency signal representations *IEEE Signal Process. Mag.* **9** 21–67

Javorka M, Lazarova Z, Tonhajzerova I, Turianikova Z, Honzikova N, Fiser B, Javorka K and Baumert M 2011 Baroreflex analysis in diabetes mellitus: linear and nonlinear approaches *Med. Biol. Eng. Comput.* **49** 279–88

Kashihara K, Kawada T, Sugimachi M and Sunagawa K 2009 Wavelet-based system identification of short-term dynamic characteristics of arterial baroreflex *Ann. Biomed. Eng.* **37** 112–28

Keissar K, Maestri R, Pinna G D, Rovere M T L and Gilad O 2010 Non-invasive baroreflex sensitivity assessment using wavelet transfer function-based time–frequency analysis *Physiol. Meas.* **31** 1021–36

La Rovere M T, Pinna G D and Raczak G 2008 Baroreflex sensitivity: measurement and clinical implications *Ann. Noninvasive Electrocardiol.* **13** 191–207

Lachaux J P, Lutz A, Rudrauf D, Cosmelli D, Quyen M L V, Martinerie J and Varela F 2002 Estimating the time-course of coherence between single-trial brain signals: an introduction to wavelet coherence *Neurophysiol. Clin.* **32** 157–74

Laude D *et al* 2004 Comparison of various techniques used to estimate spontaneous baroreflex sensitivity (the EuroBaVar study) *Am. J. Physiol. Regul. Integr. Comp. Physiol.* **286** R226–31

Li D and Jung R 2000 Quantifying coevolution of nonstationary biomedical signals using time-varying phase spectra *Ann. Biomed. Eng.* **28** 1101–15

Mainardi L T, Bianchi A M, Furlan R, Piazza S, Barbieri R, di Virgilio V, Malliani A and Cerutti S 1997 Multivariate time-variant identification of cardiovascular variability signals: a beat-to-beat spectral parameter estimation in vasovagal syncope *IEEE Trans. Biomed. Eng.* **44** 978–89

Martinez J P, Almeida R, Olmos S, Rocha A P and Laguna P 2004 A wavelet-based ECG delineator: evaluation on standard databases *IEEE Trans. Biomed. Eng.* **51** 570–81

Mateo J and Laguna P 2003 Analysis of heart rate variability in the presence of ectopic beats using the heart timing signal *IEEE Trans. Biomed. Eng.* **50** 334–43

Matz G and Hlawatsch F 2000 Time–frequency coherence analysis of nonstationary random processes *Proc. 10th IEEE Workshop Statistical Signal and Array Processing* pp 554–8

Mincholé A, Pueyo E, Rodríguez J F, Zacur E, Doblaré M and Laguna P 2011 Quantification of restitution dispersion from the dynamic changes of the T-wave peak to end, measured at the surface ECG *IEEE Trans. Biomed. Eng.* **58** 1172–82

Nollo G, Faes L, Antolini R and Porta A 2009 Assessing causality in normal and impaired short-term cardiovascular regulation via nonlinear prediction methods *Phil. Trans. R. Soc.* A **367** 1423–40

Nollo G, Faes L, Porta A, Antolini R and Ravelli F 2005 Exploring directionality in spontaneous heart period and systolic pressure variability interactions in humans: implications in the evaluation of baroreflex gain *Am. J. Physiol. Heart Circ. Physiol.* **288** H1777–85

Nowak J A, Ocon A, Taneja I, Medow M S and Stewart J M 2009 Multiresolution wavelet analysis of time-dependent physiological responses in syncopal youths *Am. J. Physiol. Heart Circ. Physiol.* **296** H171–9

Ocon A J, Medow M S, Taneja I and Stewart J M 2011 Respiration drives phase synchronization between blood pressure and RR interval following loss of cardiovagal baroreflex during vasovagal syncope *Am. J. Physiol. Heart Circ. Physiol.* **300** H527–40

Orini M, Bailón R, Mainardi L, Laguna P and Flandrin P 2011 Characterization of the dynamic interactions between cardiovascular signals by time–frequency coherence *IEEE Trans. Biomed. Eng.* **58** Early Access (http://dx.doi.org/10.1109/TBME.2011.2171959)

Pagani M, Somers V, Furlan R, Dell'Orto S, Conway J, Baselli G, Cerutti S, Sleight P and Malliani A 1988 Changes in autonomic regulation induced by physical training in mild hypertension *Hypertension* **12** 600–10

Porta A, Catai A M, Takahashi A C M, Magagnin V, Bassani T, Tobaldini E, van de Borne P and Montano N 2011 Causal relationships between heart period and systolic arterial pressure during graded head-up tilt *Am. J. Physiol. Regul. Integr. Comp. Physiol.* **300** R378–86

Robbe H W, Mulder L J, Rü, ddel H, Langewitz W A, Veldman J B and Mulder G 1987 Assessment of baroreceptor reflex sensitivity by means of spectral analysis *Hypertension* **10** 538–43

Shin Y J, Gobert D, Sung S H, Powers E J and Park J B 2005 Application of cross time–frequency analysis to postural sway behavior: the effects of aging and visual systems *IEEE Trans. Biomed. Eng.* **52** 859–68

Sörnmo L and Laguna P 2005 ECG Signal Processing: Heart Rate Variability *Bioelectrical Signal Processing in Cardiac and Neurological Applications* (Berlin: Academic) chap. 8 pp 567–631

Vallais F, Baselli G, Lucini D, Pagani M and Porta A 2009 Spontaneous baroreflex sensitivity estimates during graded bicycle exercise: a comparative study *Physiol. Meas.* **30** 201–13

Westerhof B E, Gisolf J, Karemaker J M, Wesseling K H, Secher N H and van Lieshout J J 2006 Time course analysis of baroreflex sensitivity during postural stress *Am. J. Physiol. Heart Circ. Physiol.* **291** H2864–74

Westerhof B E, Gisolf J, Stok W J, Wesseling K H and Karemaker J M 2004 Time-domain cross-correlation baroreflex sensitivity: performance on the EUROBAVAR data set *J. Hypertens.* **22** 1371–80

White L B and Boashash B 1990 Cross spectral analysis of nonstationary processes *IEEE Trans. Inf. Theory* **36** 830–5

Wiklund U, Akay M, Morrison S and Niklasson U 2002 Wavelet decomposition of cardiovascular signals for baroreceptor function tests in pigs *IEEE Trans. Biomed. Eng.* **49** 651–61

Xiao X, Mullen T J and Mukkamala R 2005 System identification: a multi-signal approach for probing neural cardiovascular regulation *Physiol. Meas.* **26** R41–71